

Superorbital variability in hard X-rays

S. A. Farrell,¹* D. Barret¹ and G. K. Skinner^{2,3}

¹*Centre d'Etude Spatiale des Rayonnements, CNRS/UPS, 9 Avenue du Colonel Roche, 31028 Toulouse Cedex 4, France*

²*CRESST and Astroparticle Physics Laboratory, Code 661, NASA/Goddard Space Flight Center, Greenbelt, MD 20771, USA*

³*Department of Astronomy, University of Maryland, College Park, MD 20742, USA*

Accepted 2008 October 29. Received 2008 October 29; in original form 2008 February 8

ABSTRACT

We present the results of a study with the *Swift* Burst Alert Telescope in the 14–195 keV range of the long-term variability of five low-mass X-ray binaries with reported or suspected superorbital periods – 4U 1636–536, 4U 1820–303, 4U 1916–053, Cyg X-2 and Sco X-1. No significant persistent periodic modulation was detected around the previously reported periods in the 4U 1916–053, Cyg X-2 or Sco X-1 light curves. The ~ 170 -d period of 4U 1820–303 was detected up to 24 keV, consistent with variable accretion due to the previously proposed triple system model. The ~ 46 -d period in 4U 1636–536 was detected up to 100 keV, with the modulation in the low- and high-energy bands found to be phase shifted by $\sim 180^\circ$ with respect to each other. This phase shift, when taken together with the near-coincident onset of the ~ 46 -d modulation and the low/hard X-ray state, leads us to speculate that the modulation could herald transient jet formation.

Key words: accretion, accretion discs – stars: neutron – X-rays: binaries.

1 INTRODUCTION

Long-term ‘superorbital’ periodic variability has been observed in soft X-rays from over 30 X-ray binaries with the All Sky Monitor (ASM) on the *Rossi X-ray Timing Explorer* (*RXTE*) satellite (see e.g. Sood et al. 2007). Also known as ‘long’ or ‘third’ periods, these modulations are defined simply as any periodic variability greater than the orbital period. This very general definition of superorbital variability is consistent with a number of physical mechanisms for the variation. Unlike binary orbital or neutron star spin periods, the mechanisms behind superorbital variability are not well understood. The precession of a warped accretion disc modulating the X-ray flux from the compact object is currently the favoured model (see e.g. Wijers & Pringle 1999; Clarkson et al. 2003a). This warp can be caused by the gravitational field of the donor star (see e.g. Larwood et al. 1996), or by radiation pressure exerted by the central X-ray emitting regions (see e.g. Wijers & Pringle 1999). Ogilvie & Dubus (2001) showed that while radiation-driven warping gives a coherent picture of superorbital periods, not all systems agree with its predictions (e.g. 2S 0114+650; Farrell et al. 2008).

Other models proposed to explain superorbital variability include variations in the accretion rate (caused by stellar pulsations of the donor star, irregular Roche lobe overflow or asymmetric stellar wind capture; Weiler et al. 1992; Psaltis 2006), precession of the neutron star spin-axis in an X-ray pulsar (Trümper et al. 1986; Stairs, Lyne & Shemar 2000), variations in the location of an accreting hotspot (Rutten, van Paradijs & Tinbergen 1992) and the presence of a third

body in the system (i.e. a triple system; Paul, Kitamoto & Makino 2000; Chou & Grindlay 2001).

While most superorbital periods are at best quasi-periodic, four X-ray binaries have been shown to exhibit stable superorbital modulation over long time-scales – Her X-1, LMC X-4, SS 433 and 2S 0114+650 (Paul & Kitamoto 2002; Sood et al. 2006). Other systems such as SMC X-1 have superorbital periods that have been observed to vary smoothly within a well-defined range (Clarkson et al. 2003a), while other superorbital periods appear to evolve stochastically. It is thus clear that there is more than one mechanism behind the superorbital modulations.

A number of X-ray binaries were regularly monitored in hard X-rays by the *Compton Gamma Ray Observatory* (*CGRO*) Burst and Transient Source Experiment (BATSE) for the first ~ 1600 d of the *RXTE* mission (Harmon et al. 2004). Since the decommissioning of *CGRO* in 2000 June, the lack of high-energy response of the *RXTE* ASM has precluded long-term studies of superorbital variability simultaneously at low and high energies. The launch of *Swift* in 2004 saw the arrival of a wide field-monitoring instrument capable of complementing the *RXTE* ASM in hard X-rays – the Burst Alert Telescope (BAT; Barthelmy et al. 2005). In this paper, we present the results of a search for the previously reported superorbital modulation of five low-mass X-ray binaries (LMXBs) in the BAT 14–195 keV light curves.

2 SOURCES

2.1 4U 1636–536

4U 1636–536 was discovered following a series of type I X-ray bursts observed with the *SAS 3* satellite (Hoffman, Lewin & Doty

*E-mail: sean.farrell@cesr.fr

1977) and later classified as an atoll source (Hasinger & van der Klis 1989). The orbital period of 3.8 h was derived from optical photometric measurements by Pedersen, van Paradijs & Lewin (1981). A distance of 4.3 ± 0.6 kpc was derived by Jonker & Nelemans (2004) using type I photospheric radius expansion bursts. However, more recent analyses by Galloway et al. (2006) derived a distance of 6.0 ± 0.5 kpc for a canonical neutron star (i.e. $M_{\text{NS}} = 1.4 M_{\odot}$, $R_{\text{NS}} = 10$ km).

Casares et al. (2006) performed phase-resolved Very Large Telescope spectroscopy of the irradiated donor in 4U 1636–536, using Doppler imaging of the N III $\lambda 4640$ Bowen transition lines to determine a new set of spectroscopic ephemerides. A reanalysis of burst oscillations using these ephemerides allowed them to place the first dynamical constraints on the masses of the binary companions, constraining the mass function [$f(M) = 0.76 \pm 0.47 M_{\odot}$], mass ratio ($q \sim 0.21$ – 0.34) and system inclination angle ($i \sim 36^{\circ}$ – 60°).

Shih et al. (2005) reported the onset of a large amplitude, statistically significant periodic modulation at ~ 46 d in the *RXTE* ASM data, interpreting this periodicity as due to an accretion rate variability related to the X-ray irradiation of the disc. These same authors noted a gradual decline in the X-ray flux of this source coincident with the appearance of the ~ 46 -d variability, arguing that 4U 1636–53 was transiting from activity to quiescence due to a reduction in the mass accretion rate. Fiocchi et al. (2006), however, observed a hard tail dominating the spectrum above 30 keV using data from the *INTEGRAL* satellite, speculating that this high-energy emission could be linked to the onset of relativistic outflows (i.e. jets).

The hard state of atoll sources has been previously considered to be associated with the presence of a steady jet and radio emission (see e.g. Fender 2006; Migliari & Fender 2006). When compared with black hole systems containing jets, Migliari & Fender (2006) found that the neutron star systems were less radio loud for a given X-ray luminosity, but that the jet power in both the classes of object scales linearly with accretion rate. Neutron star LMXBs in the low/hard state are thus expected to contain weaker radio jets than their black hole counterparts.

A number of radio observations of 4U 1636–536 were performed before the onset of the 46-d modulation, the decreased X-ray flux and the hardening of the X-ray spectrum, showing an absence of significant radio emission (see Section 6.2.4). No radio observations targeting this source after the onset of the modulation or the transition to the low/hard state have been reported in the literature. As such, the presence of jets in this system is yet to be confirmed.

2.2 4U 1820–303

4U 1820–303 was discovered near the centre of the globular cluster NGC 6624 in 1974 by the *Uhuru* satellite (Giacconi et al. 1974). The subsequent discovery of intense bursts associated with thermonuclear flashes from this source confirmed it as a LMXB containing a neutron star, making this the first identified source of type I X-ray bursts (Grindlay et al. 1976). A distance of 7.6 ± 0.4 kpc has been estimated using the bursts as a standard candle (Kuulkers et al. 2003).

The system consists of a white dwarf and a neutron star orbiting their common centre of mass with an orbital period of 11.4 min (Rappaport et al. 1987; Stella, Friedhorsky & White 1987). Hasinger & van der Klis (1989) later classified 4U 1820–303 as an atoll source, with Zhang et al. (1998) observing the presence of kHz quasi-periodic oscillations (QPOs). Bloser et al. (2000b) observed that the QPO frequency was strongly correlated with the position

on the colour–colour diagram. This result (in combination with the observed saturation of the QPO frequency at high accretion rates) lead them to conclude that they were observing the last stable orbit in the accretion disc.

Priedhorsky & Terrell (1984b) noted a periodic ~ 170 -d variability in the X-ray flux, over which time-scale the source moves from the soft/banana state to the hard/island state. This quasi-periodic ~ 170 -d variability was later proposed to be a result of variable mass accretion due to tidally induced modulation of the orbital eccentricity by a third massive body (Chou & Grindlay 2001). Recently, Tarana et al. (2007) reported the detection of a hard X-ray tail above 50 keV from this source in the island state, concluding that this emission is likely due either to emission of non-thermal electrons or thermal emission from plasmas with a relatively high temperature.

Zdziarski, Wen & Gierliński (2007a) performed an analysis of the superorbital modulation using *RXTE* ASM data. These authors undertook a study of hierarchical triple system models yielding the required quasi-periodic eccentricity oscillations, finding that the resulting theoretical light curves matched well with the observed ones. Zdziarski et al. (2007b) reported a dependence on the X-ray spectral state of both the depth and phasing of the orbital X-ray modulation. This led them to favour a model in which the observed X-ray modulation is caused by scattering in hot gas around an accretion-stream bulge at the disc edge; as the mass accretion rate changes with the ~ 170 -d cycle, so the size and location of this bulge varies. The average flux calculated over the course of the superorbital variability was found to be compatible with the model of accretion due to the angular momentum loss via emission of gravitational radiation.

2.3 4U 1916–053

4U 1916–053 was discovered in 1974 by the *Uhuru* satellite (Giacconi et al. 1974) and is the most compact X-ray binary to exhibit periodic intensity dips. Type I X-ray bursts each lasting ~ 10 s have been observed from this source with a recurrence time-scale of several hours (Becker et al. 1977; Lewin et al. 1977). A distance of 8.8 ± 1.3 kpc has been estimated by Jonker & Nelemans (2004) from photospheric radius expansion during the bursts. 4U 1916–053 is classified as an atoll source and displays a similar path in the X-ray colour–colour diagram to 4U 1820–303, although with significantly lower luminosity (Bloser et al. 2000a).

The X-ray dips have been ascribed to obscuration of the X-ray emitting region by a bulge in the outer accretion disc where the accretion stream meets the disc (White & Swank 1982). The dip recurrence period of ~ 3000 s is the shortest among the known dipping sources (Swank, Taam & White 1984). The optical counterpart was discovered as a $V = 21$ mag optical star modulating at a period of 3027.5 s by Grindlay et al. (1988). This optical period is ~ 1 per cent longer than the X-ray dip period, raising the question as to which of the values indicated the orbital period.

A 3.9-d beat period between the optical and X-ray periods was reported by Grindlay (1992), manifesting as a modulation of the X-ray dip shape (Chou, Grindlay & Bloser 2001). Timing analyses of *RXTE* PCA data and quasi-simultaneous optical data performed by Chou et al. (2001) lead them to conclude that the X-ray dip period was indeed the binary orbital period, with the slightly longer optical period produced through beating between the orbital period and the 3.9-d period, which they ascribed to the precession period of the accretion disc. They also set an upper limit of 2.06×10^{-11} s s $^{-1}$ on the $|\dot{P}|$, arguing that the inferred stability and the partial

clustering of X-ray bursts preceding the X-ray dips continues to suggest that the system may be a hierarchical triple.

A regular long-term periodicity of 199 d (and a possible period of 40.6 d) was reported in the X-ray flux using data from the *Vela 5B* satellite by Priedhorsky & Terrell (1984a), which the authors ascribed to disc precession. Later analysis of the same data by Smale & Lochner (1992) found that the 199-d modulation was not very strong, with a confidence level of just 80 per cent. Homer et al. (2001) analysed ~ 3.7 yr of *RXTE* ASM data, finding no significant peaks above the red or white noise levels at any period. Šimon (2005) investigated the long-term X-ray activity of 4U 1916–053 using 7 yr of *RXTE* ASM data, finding that a cycle of about 230–250 d occurred only in a limited time interval, materializing as variations of the recurrence time and amplitude of outbursts. Šimon (2005) also concluded that the movement of 4U 1916–053 along the atoll path in the X-ray colour–colour diagram during the outbursts implied that the observed long-term variability was caused by variable accretion on to the neutron star, and not by disc precession (which would imply occultation and/or absorption effects). A more recent analysis of 8.5 yr of *RXTE* ASM data by Wen et al. (2006) failed to detect any long-term periodic variability.

2.4 Cyg X-2

Cyg X-2 is one of the six Galactic LMXBs that are classified as Z-sources (Hasinger & van der Klis 1989), and was first discovered by Byram, Chubb & Friedman (1966) with a sounding rocket experiment. Type I X-ray bursts were reported by Smale (1998), confirming a neutron star as the compact object. Distances of 7.2 ± 1.1 and 13 ± 2 kpc have been estimated from optical observations (Orosz & Kuulkers 1999) and photospheric radius expansion in the bursts (Jonker & Nelemans 2004), respectively. A binary orbital period of 9.8444 d was deduced from the optical behaviour of the donor star (Casares, Charles & Kuulkers 1998). A high-energy tail has been observed in the X-ray spectrum during a number of observations (Di Salvo, Robba & Stella 2002; Piraino, Santangelo & Kaaret 2002; Lavagetto et al. 2006), although hard X-ray emission does not appear to be a constant feature of this source (Lavagetto et al. 2006).

A 77-d periodicity in data from the *Vela 5B* satellite was reported by Smale & Lochner (1992). Wijnands, Kuulkers & Smale (1996) reported the detection of a 78-d period in *RXTE* ASM data from the first 160 d of the mission, and showed that their result was supported by archival data from the *Ariel 5* and *Vela 5B* missions. However, analyses of archived data from the all sky monitors on the *RXTE*, *Ginga*, *Ariel 5* and *Vela 5B* satellites and the scanning modulation collimator of *HEAO 1* by Paul et al. (2000) found no evidence for a stable modulation in the X-ray emission. Strong peaks at 40.4 and 68.8 d in the *RXTE* ASM data, and at 53.7 and 61.3 d in the *Ginga* ASM data were observed by these authors, leading them to conclude that the superorbital variability in this system (if real) is aperiodic. Dynamic analyses performed on 7 yr of *RXTE* ASM data by Clarkson et al. (2003b) revealed complex quasi-periodic behaviour, with a highly significant periodicity at ~ 59 d in a 300 d section of the light curve, with significant recurring features at ~ 40 d appearing sporadically.

2.5 Sco X-1

The Z-source Sco X-1 was the first X-ray binary discovered and is the brightest persistent extrasolar X-ray source (Giacconi et al.

1962). Although the system properties are consistent with it containing a neutron star with a weak magnetic field, no type I bursts have been observed so far (Mirabel & Rodrigues 2003). Radio emission from the vicinity of Sco X-1 was first reported by Andrew & Purton (1968), with later high-resolution radio interferometry unveiling compact jets through the formation of twin radio lobes with variable morphology (Fomalont, Geldzahler & Bradshaw 2001). A distance of 2.8 ± 0.3 kpc was determined from trigonometric parallax (Bradshaw, Fomalont & Geldzahler 1999). The orbital period of ~ 18.9 h was originally discovered in 85 yr of archived photometric optical data by Gottlieb, Wright & Liller (2001), and more recently observed in X-rays by Vanderlinde, Levine & Rappaport (2003).

A high-energy tail above 30 keV in the X-ray spectrum was observed in *CGRO* Oriented Scintillation Spectrometer Experiment (OSSE) data by Strickman & Barret (2000) and later verified in *RXTE* and *INTEGRAL* data by D’Amico et al. (2001) and Di Salvo et al. (2006), respectively. A periodic modulation at 37 d was reported by Peele & White (1996) in nine months of *RXTE* ASM data, although this modulation has yet to be confirmed.

3 DATA REDUCTION

While awaiting gamma-ray bursts, the *Swift* BAT instrument accumulates data in survey mode. A given source is within the field of view of the BAT ~ 10 per cent of the time, with a typical integration time per pointing of around 1000 s. Standard software was used to extract and clean ‘detector plane images’ in four energy bands for each ‘observation’ (typically a few thousand seconds, often comprising several shorter segments) and to calculate the arrays of weights corresponding to the visibility of each source within the field of view by each detector pixel during that observation. A program developed for the purpose by the authors was then used to fit simultaneously the intensities of the sources and a series of background model components (equivalent functionality to that provided by this program is now available in the latest public software, though the public software was not available at the time the analyses were performed). Corrections were applied for Earth occultation and the known energy-dependent variation of the instrument sensitivity with off-axis angle.

4 DATA ANALYSIS

The BAT 14–24 keV (A), 24–50 keV (B), 50–100 keV (C) and 100–195 keV (D) light curves were used for these analyses, rebinned at 1 d. The average sampling rate for the reduced light curves prior to rebinning varied from ~ 0.8 to 12.5 d $^{-1}$. For comparison, the *RXTE* ASM 1.5–12 keV 1 d average light curves for the same time-span were analysed to cover the low energy range of the spectrum. The 1-d binning was chosen for convenience as we were interested only in the long-term variability of the target sources. Table 1 lists the number of data points and average sampling frequencies for the BAT and *RXTE* ASM light curves for each source.

All data points were weighted using the modified weighting scheme developed by Corbet, Markwardt & Tueller (2007). In this method, individual data points are given weights based on both the non-uniform measurement uncertainties and the intrinsic source variability. The resulting weighted count rate R'_i is given by

$$R'_i = \frac{R_i}{[(f\sigma_i)^2 + V_s]}, \quad (1)$$

where R_i is the raw unweighted rate, f is a correction factor to account for underestimation of the error on each point and σ_i is the

Table 1. Swift BAT and *RXTE* ASM light curve properties for each of the five sources analysed.

Source	<i>RXTE</i> ASM		BAT A		BAT B		BAT C		BAT D	
	N^a	f_{samp}^b	N	f_{samp}	N	f_{samp}	N	f_{samp}	N	f_{samp}
4U 1636–536	481	0.77	483	0.78	485	0.78	485	0.78	494	0.80
4U 1820–303	452	0.72	419	0.75	405	0.72	426	0.76	429	0.76
4U 1916–053	485	0.78	379	0.69	384	0.70	386	0.70	390	0.71
Cyg X-2	570	0.91	504	0.81	493	0.79	507	0.81	507	0.81
Sco X-1	485	0.77	483	0.77	470	0.75	466	0.74	465	0.74

^aNumber of points in the light curve.^bAverage light-curve sampling frequency in units of d^{−1}.

uncertainty for the point. V_s is the estimated variance due to source variability, given by

$$V_s = \frac{\sum_{i=1}^N (\bar{R} - R_i)^2}{N-1} - \frac{\sum_{i=1}^N (f\sigma_i)^2}{N}, \quad (2)$$

where \bar{R} is the mean count rate and N is the number of data points in the light curve.

The f factor was derived for each of the energy bands in the BAT and *RXTE* ASM light curves by fitting a constant to the light curves of a source expected to be stable. The f factor was determined by taking the square root of the reduced χ^2 value obtained from fitting data from the Crab (Corbet, private communication). For cases in which the V_s parameter was negative (applicable to sources which are very faint in the given energy band), V_s was set to zero and the method reverts to the ‘simple’ weighting technique proposed by Scargle (1989).

Power spectra were generated for each of the weighted light curves using the fast periodogram *FASPER* subroutine of the Lomb–Scargle periodogram (Lomb 1975; Scargle 1982; Press & Rybicki 1989). The oversampling and high-frequency factors – which set the period range and resolution (Press & Rybicki 1989) – were both set at two for each analysis run, allowing us to search for periodic variability in the ~ 1.3 –1000 d range. The Lomb–Scargle technique allows us to sample below the average Nyquist period (with reduced sensitivity) due to the unevenly sampled nature of the data, without creating problems due to aliasing as would be seen in the analysis of an evenly sampled data set using standard fast Fourier techniques. The frequency range and binning were chosen to give a good coverage of the range covered by known superorbital periods while at the same time providing sufficient resolution in the power spectra. The 99 per cent white noise significance levels were estimated using Monte Carlo simulations (see e.g. Kong, Charles & Kuulkers 1998). The 99 per cent red noise significance levels were estimated using the *REDFIT* subroutine,¹ which fits a first-order autoregressive process to the time series in order to estimate the red-noise spectrum (Schulz & Mudelsee 2002).

5 RESULTS

5.1 4U 1636–536

Fig. A1 shows the *RXTE* ASM and *Swift* BAT light curves for 4U 1636–536 while Fig. B1 shows the power spectra. The previously reported 46-d periodicity is clearly detected in the *RXTE* ASM 1.5–12 keV data, and is also significantly present in the BAT 14–24, 24–50 and 50–100 keV light curves. No significant modulation

above 100 keV is detected in the 1.3–1000 d range. In order to investigate the likely origin of the 46-d modulation, the raw (i.e. unweighted) *RXTE* ASM, BAT A, BAT B and BAT C light curves were each folded over the 46-d period, setting phase zero arbitrarily to the start of the BAT light curves at MJD 53360. The profile of the modulation was observed to shift in phase between the 1.5–12 and 14–24 keV energy bands, so that the profiles above 14 keV are almost 180° out of phase with the lower energy modulation (Fig. 1).

It can be clearly seen in Fig. A1 that the period of the modulation is not stable, with the time between successive peaks varying over time. In order to test how the drift in the period affects the width of the peak in the power spectra, we simulated light curves with the same sampling as the *RXTE* ASM, BAT A, BAT B and BAT C light curves with a stable sinusoidal modulation with a period

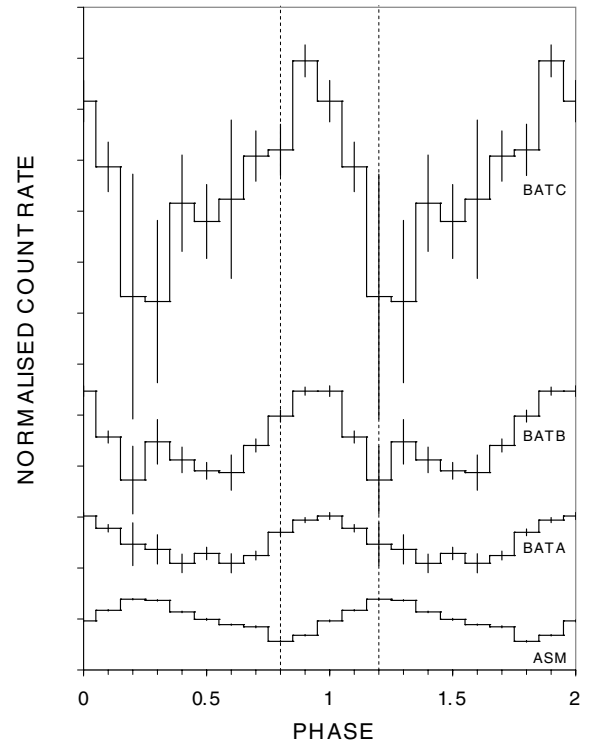


Figure 1. The light curves of 4U 1636–536 folded over the 46-d period. From bottom: *RXTE* ASM 1.5–12 keV profile, BAT A 14–24 keV profile, BAT B 24–50 keV profile and BAT C 50–100 keV profile. The vertical dashed lines indicate the phases corresponding to the minimum and maximum of the *RXTE* ASM profile. The count rates are normalized to the mean of each light curve and the scale for each profile is the same.

¹ http://ftp.ncdc.noaa.gov/pub/data/paleo/softlib/redfit/redfit_preprint.pdf

of 46 d. Power spectra were then generated and compared with those produced using the real data shown in Fig. B1. In all cases, the peaks in the real power spectra were marginally wider than the simulated spectra. While this discrepancy could possibly be linked to the change in the period, the difference could also be due to the effects of noise or statistical scatter.

Analysis of the BAT light curves prior to rebinning into 1 d average data sets found an additional peak at ~ 77 above the 99 per cent white noise significance levels. Farrell, O'Neill & Sood (2005) have shown that by imposing a known periodic sampling rate, any spurious peaks in the power spectrum produced by aliasing or spectral leakage should be shifted to other frequencies. By simulating light curves with periodic modulations at 46 and 77 d with the same sampling as the BAT data, we found that rebinning the light curves should increase the significance of a real peak. The significance of the 77-d peak was dramatically reduced in power spectra of the rebinned BAT light curves (see Fig. B1) and is well below the dominant 99 per cent white noise significance levels. We thus identify the 77-d peak as spurious.

5.2 4U 1820–303

Fig. A2 shows the *RXTE* ASM and *Swift* BAT light curves for 4U 1820–303 while Fig. B2 shows the power spectra. The previously reported ~ 170 -d periodicity is clearly detected in the *RXTE* ASM 1.5–12 keV data as a single broad peak, and is also significantly present in the BAT 14–24 keV light curves. No peaks around 46 d are significantly present in the 24–195 keV power spectra. The 1.5–12 and 14–24 keV light curves were thus epoch folded over the 170-d period, setting phase zero arbitrarily to the start of the ASM light curve at MJD 53353. The count rates were normalized to the mean rate (Fig. 2). Unlike 4U 1636–536, no phase shift was observed between the low- and high-energy profiles.

The period of the superorbital modulation of 4U 1820–303 has been known to vary over time (Zdziarski et al. 2007a). As such, to test the effect of a varying period on the width of the peak in the power spectra, we simulated light curves with a stable sinusoidal modulation at 170 d with the same sampling as the *RXTE* ASM and BAT A light curves. We then generated power spectra for the simulated light curves and compared them with the power spectra shown in Fig. B2. As with 4U 1636–536, the peaks in the real power spectra were marginally wider than those generated using the simulated data. While this discrepancy could again be linked to a changing period, there is no more than a suggestion of possible slight broadening of the peaks.

The simulations clearly show that the width of the peak is a function of both the period of the modulation and the number of cycles in the data set. Therefore, in order to compare the width of the superorbital peak in the 4U 1820–303 power spectra with that of 4U 1636–536, this relationship needs to be taken into account. We thus took the full width of the peaks at 50 per cent of the maximum power, normalized it by the period of the modulation and then multiplied it by the number of cycles in the light curves. Comparing the normalized peak widths shown in Table 2, we see that the values for the real peaks are comparable for both 4U 1636–536 and 4U 1820–303, and are consistently marginally greater than the width of the simulated peaks.

In addition to the ~ 170 -d modulation, a peak at around ~ 100 d marginally exceeds the 99 per cent white noise significance level in the 24–50 keV power spectrum. However, the lack of a significant peak at this period in the other BAT power spectra (in particular between 14 and 24 keV) leads us to conclude that this peak is

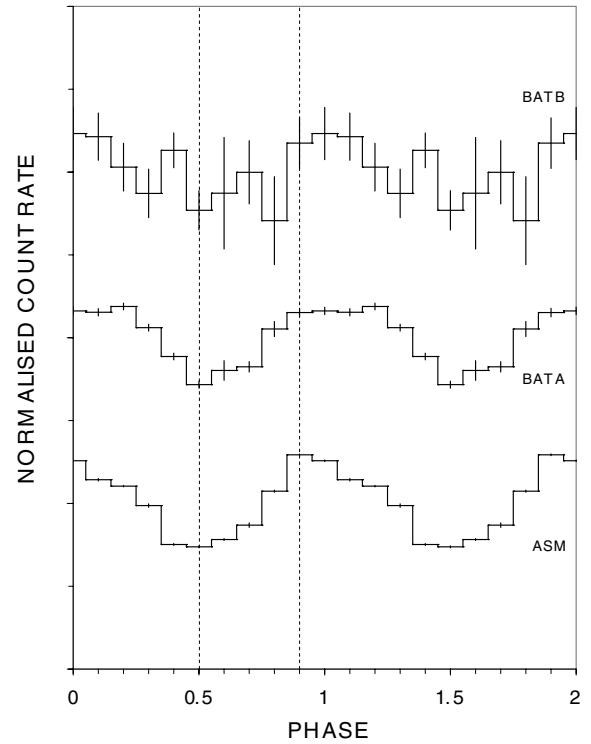


Figure 2. The light curves of 4U 1820–303 folded over the 170-d period. From bottom: *RXTE* ASM 1.5–12 keV profile, BAT A 14–24 keV profile and BAT B 24–50 keV profile. The vertical dashed lines indicate the phases corresponding to the minimum and maximum of the *RXTE* ASM profile. The count rates are normalized to the mean of each light curve and the scale for each profile is the same.

Table 2. Comparison between the normalized widths of the superorbital peaks in real and simulated power spectra for 4U 1636–536 and 4U 1820–303.

Data set	4U 1636–536		4U 1820–303	
	W_{real}	W_{sim}	W_{real}	W_{sim}
<i>RXTE</i> ASM	0.94	0.82	1.11	0.90
BAT A	1.07	0.88	0.94	0.86
BAT B	0.97	0.88	–	–
BAT C	1.00	0.88	–	–

spurious. No other significant modulation above 50 keV is detected in the 1.3–1000 d range.

5.3 4U 1916–053

Fig. A3 shows the *RXTE* ASM and *Swift* BAT light curves for 4U 1916–053 while Fig. B3 shows the power spectra. No significant modulation in any of the light curves is apparent in the 1.3–1000 d range, indicating that either the 199- and 40.6-d periodicities detected by Priedhorsky & Terrell (1984a) were spurious, the mechanism for these modulations was not active during the time of our observations, or that the signal was not sufficiently stable and/or persistent over the entire observing window for it to be detected in a single power spectrum.

The power spectrum of the *RXTE* ASM data for 4U 1916–053 appears to be dominated by white noise. This result is in contrast to

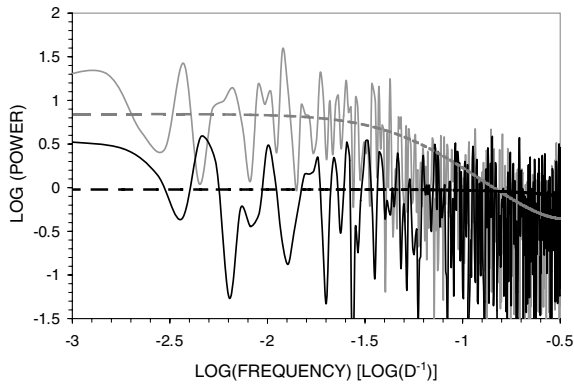


Figure 3. Log-log power spectra of the 1.5–12 keV *RXTE* ASM light curves of 4U 1916–053 covering the Homer et al. (2001) time frame (grey solid lines) and the time frame covered by the BAT data (black solid lines). The red noise models for each power spectrum are plotted as dashed lines for comparison.

the results of Homer et al. (2001), who found that red noise dominated the power spectrum of the first four years of *RXTE* ASM data. Analysis of the Homer et al. (2001) data using our analysis methods confirm that red noise was indeed dominant in the *RXTE* ASM data, but has since dropped in significance. Fig. 3 presents a comparison between the power spectra generated for the *RXTE* ASM data covering the Homer et al. (2001) epoch (MJD 50150–51500) and the time-span used for our analyses (MJD 53360–53900), clearly showing the drop in red noise.

5.4 Cyg X-2

Fig. A4 shows the *RXTE* ASM and *Swift* BAT light curves for Cyg X-2 while Fig. B4 shows the power spectra. A strong, broad peak at ~ 190 d is present in the *RXTE* ASM 1.5–12 keV and BAT 14–24 keV power spectra. These peaks are located at approximately 0.5 yr, a common location for spurious peaks (see e.g. Farrell et al. 2005). No other significant peaks are present in any of the energy bands. A peak at ~ 40 d is present in the power spectrum from the *RXTE* ASM data, similar to the 40.4-d signal detected by Paul et al. (2000). Although the power of this peak exceeds the 99 per cent white noise significance level, it is well below the red noise significance level.

5.5 Sco X-1

Fig. A5 shows the *RXTE* ASM and *Swift* BAT light curves for Sco X-1 while Fig. B5 shows the power spectra. No periodic variability greater than the dominant 99 per cent white noise significance level is present in the *RXTE* ASM or BAT power spectra in the 1.3–1000 d range.

6 DISCUSSION

The typical shape of the X-ray spectrum for LMXBs consists of a thermal Comptonization component (sometimes empirically modelled as a power law with exponential cut-off) curtailed at low energies by photoelectric absorption, often with the addition of a low-energy blackbody component arising either from thermal emission from the inner regions of the disc or very close to the surface of the neutron star (see e.g. Bloser et al. 2000b; Barret 2001, for

a review). In the low/hard state, an additional power-law component is sometimes required in order to model the hard X-ray tail (see e.g. Tarana et al. 2007), with the hard X-ray emission attributed variously to Comptonization by high-temperature thermal or non-thermal electrons in the accretion disc corona or in compact jets.

6.1 The ~ 170 -d period in 4U 1820–303

The ~ 170 -d period in 4U 1820–303 has been attributed to variable accretion linked to the presence of a third body in this system, whereby the eccentricity of the inner orbit is modulated by tidal effects produced by the outer body (Chou & Grindlay 2001; Zdziarski et al. 2007a). Transitions between the high/soft and low/hard states over this time-scale are linked to variability in the accretion rate (Bloser et al. 2000b) and the movement in and out of the inner region of the accretion disc (see e.g. Malzac 2007), thus modulating the thermal Comptonization region of the spectrum. This thermal Comptonization component has been seen to dominate the spectrum up to ~ 50 keV, above which 4U 1820–303 has only been detected on one occasion during the low/hard (island) state, during which a high-energy non-thermal tail was found to dominate (Tarana et al. 2007).

The ~ 170 -d period has been seen to correspond to normal atoll source motion in the colour–colour diagram, with the minimum of the modulation coinciding with the transition to the island state (Bloser et al. 2000b). If the appearance of the high-energy non-thermal tail is regular and tied to the island state (and thus the minimum of the superorbital modulation), a hardening of the spectrum would be anticipated every ~ 170 d. We would therefore expect to detect the modulation above 50 keV, anticorrelated with the low-energy modulation. If the hard tail in 4U 1820–303 preferentially appears on a regular basis during the transition to the island state, we would also expect the low- and high-energy modulations to be out of phase. However, as mentioned in Section 5.2, no such phase shift is apparent in the folded profiles (Fig. 2).

The superorbital period should be present at least up to the 50 keV threshold, as a varying accretion rate would be expected to modulate the entire thermal Compton region of the spectrum. To test whether 4U 1820–303 would be detected by the BAT above 24 keV, we simulated spectra (1000 s integration times) using the BAT response files for the various island state spectral models applied to *RXTE* and *INTEGRAL* data by Bloser et al. (2000b) and Tarana et al. (2007), respectively.

Flux upper limits during the minimum of the ~ 170 -d modulation (i.e. the island state) in the three BAT energy bands above 24 keV were calculated for each of the Bloser et al. (2000b) and Tarana et al. (2007) island state spectral models. Table 3 lists the derived flux upper limits in the BAT B, C and D energy bands for each of the Bloser et al. (2000b) and Tarana et al. (2007) models. The projected flux in each band for each spectral model was also calculated, with the normalization parameters set so that the 14–24 keV model count rate equalled the measured rate in this band (the only BAT band in which we can be certain 4U 1820–303 was detected).

In all cases except the Tarana et al. (2007) simple Comptonization and the Bloser et al. (2000b) cut-off power law + disc blackbody models, the expected flux was far in excess of the derived upper limits in the 24–50 and 50–100 keV bands. Thus, within the uncertainties of this method, the non-detection of the ~ 170 -d modulation above 24 keV is most consistent with the softest island state spectral models in Tarana et al. (2007) and Bloser et al. (2000b).

Table 3. Derived flux upper limits for 4U 1820–303 in the island state in the BAT B, C and D energy bands using the model parameters in Bloser et al. (2000b) and Tarana et al. (2007).

BAT energy band	Flux upper limits ($\times 10^{-11}$ erg cm $^{-2}$ s $^{-1}$)				
	CPL + BB ^a	CompTT + BB ^b	CPL + DBB ^c	CompTT ^d	CompTT + PL ^e
B (24–50 keV)	5.5	5.5	5.2	4.8	5.5
C (50–100 keV)	1.5	1.5	1.6	1.6	1.7
D (100–195 keV)	7.4	7.0	7.6	7.9	8.6

^aCut-off power law plus blackbody model (Bloser et al. 2000b).

^bThermal Comptonization plus blackbody model (Bloser et al. 2000b).

^cCut-off power law plus disc blackbody model (Bloser et al. 2000b).

^dThermal Comptonization model (Tarana et al. 2007).

^eThermal Comptonization plus power-law model (Tarana et al. 2007).

6.2 The ~46-d period in 4U 1636–536

6.2.1 Formation of compact jets?

Fiocchi et al. (2006) linked the recent reduction in X-ray flux and the appearance of a high-energy tail in the spectrum of 4U 1636–536 to the onset of jet formation. Interestingly, the 46-d modulation first appears in the *RXTE* ASM data around the same time as this transition to the low/hard state. Fig. 4 shows the coarse binned *RXTE* ASM light curve up to MJD 53900 for 4U 1636–536 with the signal-to-noise ratio (S/N) of the 46-d peak (as taken from overlapping power spectra generated from 600 d light curve sections with a 100 d overlap). The significance of the modulation can clearly be seen to increase markedly with the decrease in flux (the significance of the 46-d periodicity did not exceed the 99 per cent significance levels until a S/N of ~ 7 was reached). The appearance of a high-energy power-law tail in the spectrum in conjunction with the first detection of the 46-d period and the reduction in flux implies a link between the three phenomena. If the assertion made by Fiocchi et al. (2006) is correct (that the transition to the low/hard island state is linked to jet formation), the 46-d modulation could be tied to transient jet formation or possibly to the precession of jets (linked, in turn, to the precession of a warped disc) in a similar fashion as seen in SS 433 (Margon 1984).

As mentioned in Section 5.1, the ~46-d modulation is clearly seen in each of the folded profiles shown in Fig. 1, with the phase of the modulation shifting with increasing energy so that the BAT C (50–100 keV) profile is almost 180° out of phase with the *RXTE*

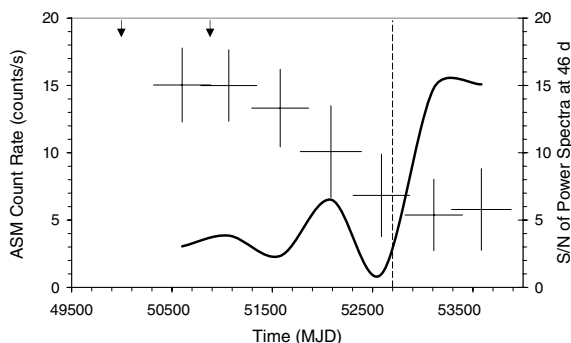


Figure 4. Average *RXTE* ASM 1.5–12.0 keV count rates (crosses) from 4U 1636–536 compared with the signal-to-noise ratio of the 46-d peak in the power spectra (solid line). The arrows indicate the times of two previous radio observations made with the ATCA, while the dashed line indicates the timing of the *INTEGRAL* observations which first detected the high-energy tail in the X-ray spectrum.

ASM (1.5–12 keV) profile. A similar phase shift was observed between the *RXTE* ASM and *INTEGRAL* light curves by Shih et al. (2005), which was attributed to the high- and low-energy modulations originating at different locations. In comparison, the profiles of the light curves of 4U 1820–303 when folded over the 170-d period show no such phase shift (Fig. 2).

6.2.2 Interpreting the phase shift

The detection of the 46-d modulation in both the high- and low-energy realms of the spectrum indicates that both the thermal and non-thermal components are varying over this time-scale. The phase shift of the modulation is inconsistent with the standard warped precessing disc model for superorbital variability, as periodic obscuration or reflection would be expected to cause the high- and low-energy modulations to vary in phase. We interpret this phase shift as an indication that the 46-d modulation arises from two separate (yet closely linked) phenomena. If the low-energy modulation seen in the *RXTE* ASM light curves is indeed due to variable obscuration of the central emission region (either the inner regions of the disc or the neutron star itself), and the high-energy modulation seen in the BAT data is a result of a varying viewing geometry of the beamed emission from the jet, it is possible to see two similar modulations in different energy bands that are out of phase. In this scenario, the jet column will be pointing towards us at roughly the same time as the bulge in the disc is obscuring the central emission region. Thus, we would see an increase in the high-energy flux at the same time as a decrease in the low-energy flux (as observed in the *RXTE* ASM and BAT data), with the high- and low-energy flux varying smoothly as the disc and jet precess together.

Many systems which show superorbital modulation ascribed to disc precession do not show any evidence for jet formation, and in some cases jet formation is inhibited due to the presence of a highly magnetized neutron star (e.g. Her X-1). However, if a warped precessing disc is present, any jets which form would expect to be coupled to the warped disc and should themselves precess. The jet would be aligned with the normal axis of the inner disc, so the scenario in which the bulge is phased to obscure the inner disc at the precise time as the jet points towards us is unlikely.

6.2.3 Transient jet formation?

A somewhat simpler explanation would be that the 46-d modulation is linked to periodic transitions between the high/soft and low/hard states, leading to transient jet formation. In this alternate scenario, the inner region of the disc moves in as the accretion rate intensifies,

resulting in an increase in the flux of seed photons and therefore an enhancement in the thermal Comptonization (i.e. soft) component of the spectrum. In this high/soft state, the conditions are not believed to be sufficient for jet formation: the disc is thought to be geometrically thin yet optically thick, with a relatively small corona as most of the accretion power is believed to be dissipated in the disc itself (see e.g. Malzac 2007). The hard region of the spectrum during this state is characterized by a weak, steep power law, generally interpreted as inverse-Compton up-scattering of soft photons by non-thermal electrons in the corona (see e.g. Barret 2001). As the accretion rate decreases, the inner regions of the disc move further out and the disc cools, becoming geometrically thick yet optically thin. In this state, most of the accretion power is believed to be transported into the corona, which in turn is thought to power the compact jet. The soft thermal component from the disc decreases as the flux of seed photons lessens, and the strong hard non-thermal component appears in conjunction with the jets. Thus, an anticorrelation between the hard and soft X-ray flux would result with both fluxes modulated over the ~ 46 d period. In this scenario, the 46-d period would represent the characteristic time-scale between disruption and recovery of the disc.

6.2.4 Searching for radio emission

Recently, Migliari et al. (2007) showed there to be a direct link between radio jet emission and the X-ray state in the neutron star X-ray binary GX 17+2. They also showed that the presence of a hard X-ray tail was coupled to the low/hard X-ray state, implying a link between the presence of radio jets and the appearance of the hard tail in the spectrum. Thus, if transient jet formation linked to spectral state transitions is the cause of the 46-d period, we would expect radio emission from this source to be modulated in phase with the hard X-ray modulation, as the jets form and radio emission ensues (see e.g. Corbel et al. 2003).

A review of the Australian Telescope Compact Array (ATCA) online archive (ATOA) shows that two previous radio observations of 4U 1636–536 were performed on 1995 September 2 and 1998 April 4, with upper limits of 0.12 and 0.15 mJy derived at 4.8 and 8.6 GHz, respectively (Berendsen et al. 2000). Both observations were performed during the high/soft state, when compact jets and resulting radio emission would not be expected. More recent observations were performed with the ATCA on 2007 June 29, 30 and July 1 as part of a multiwavelength collaboration to study LMXBs of all kinds at various epochs.² While these data are still proprietary, the principal investigator of these observations was kind enough to communicate the preliminary results; a 3σ upper limit of ~ 0.6 mJy was derived at 8.6 GHz (Dickey, private communication).

The 2–10 keV X-ray flux in the low/hard state measured with *INTEGRAL* was $\sim 1 \times 10^{-9}$ erg cm $^{-2}$ s $^{-1}$ (Fiocchi, private communication), giving a luminosity of $\sim 2 \times 10^{36}$ erg s $^{-1}$ for a distance of 4.3 kpc (Jonker & Nelemans 2004) and $\sim 4 \times 10^{36}$ erg s $^{-1}$ for a distance of 6 kpc (Galloway et al. 2006). According to the X-ray/radio luminosity correlation for neutron star LMXBs derived by Migliari & Fender (2006), 4U 1636–536 should thus have a radio luminosity (from measurements around 8.5 GHz) of somewhere between $(3\text{--}20) \times 10^{28}$ erg s $^{-1}$. The 8.5 GHz flux density would thus be ~ 1 mJy, barely sufficient for a detection to be made in the recent ATCA observations.

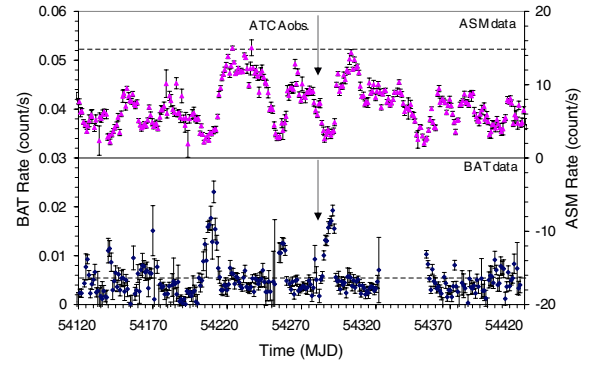


Figure 5. *RXTE* ASM (top panel) and BAT 14–50 keV (bottom panel) light curves covering MJD 54220–54420, showing the timing of the recent ATCA observations of 4U 1636–536 (arrows), which took place just prior to the transition to the low/hard island state. The dashed horizontal lines indicate the average BAT count rate and the average high/soft state count rate in the *RXTE* ASM. The latter line shows that the source re-enters the high/soft state at the peak of the ~ 46 -d modulation in the soft X-ray band.

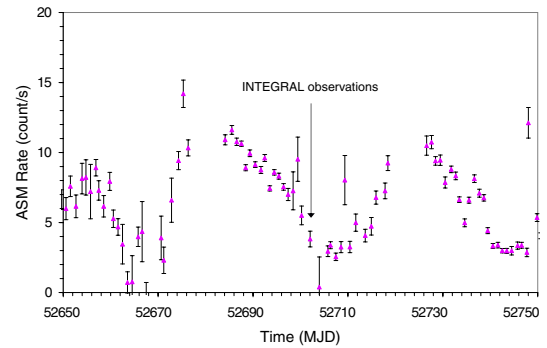


Figure 6. The *RXTE* ASM light curve of 4U 1636–536 covering MJD 52650–52750, showing the timing of the *INTEGRAL* observations (arrow) which detected the hard X-ray tail. These observations took place during the drop in low-energy flux, which presumably coincided with a rise in the high-energy flux. As the observations took place after the decommissioning of *CGRO* and prior to the launch of *Swift*, long-term monitoring data in hard X-rays are not available during this epoch.

Comparing the timing of these recent observations with the *RXTE* ASM 1.5–12 keV and the BAT 14–50 keV light curves (Fig. 5) shows that they occurred just after the maximum of the modulation in the soft X-ray band, and just before the increase in hard X-ray flux. These observations thus appear to have been performed before the transition to the low/hard state and the predicted phase of jet formation. Further support for this theory is obtained when the timing of the *INTEGRAL* observations – during which the hard tail was detected by Fiocchi et al. (2006) – is compared with the soft X-ray *RXTE* ASM light curve (Fig. 6). It can clearly be seen that the detection of the hard tail occurred during the minimum of the soft X-ray modulation, at the same time as we would have expected to see a peak in the BAT hard X-ray light curve had monitoring data been available during this epoch.

6.3 Non-detections

No evidence for the previously reported superorbital periods in 4U 1916–053, Cyg X-2 or Sco X-1 was found in the *RXTE* ASM or any of the BAT light curves. The power spectra were

² <http://www.cfa.harvard.edu/twiki/bin/view/GreatObs/JetsDisks>

instead dominated by low-frequency noise, with no peaks that would indicate the presence of real long-term periodic modulation. The modulations for 4U 1916–053 and Cyg X-2 were originally reported using *Vela 5B* data, with later analyses by Wen et al. (2006) of 8.5 yr of *RXTE* ASM data finding no significant stable modulation from either source. The detection of superorbital modulation in Sco X-1 was reported using only the first nine months of *RXTE* ASM data. It is thus apparent that either the reported detections were spurious, the mechanisms behind the superorbital variability in each of these three systems have since ceased, or the modulation does not persist over a sufficient fraction of the observing window to be detectable by our techniques. Unfortunately, the BAT light curves do not cover a sufficiently long epoch for us to subdivide the light curves, thus precluding dynamic analyses to search for signals that are potentially transient or variable in frequency.

7 CONCLUSIONS

We have analysed the *RXTE* ASM and *Swift* BAT light curves in the 1.5–195 keV range for 4U 1636–536, 4U 1820–303, 4U 1916–053, Cyg X-2 and Sco X-1. We found no evidence for periodic variability at the previously reported superorbital periods from 4U 1916–053, Cyg X-2 or Sco X-1 in either the *RXTE* ASM or BAT data. In contrast, the ~ 170 -d period in 4U 1820–303 is clearly detected up to 24 keV, consistent with the modulation arising from variable accretion due to tidal effects from the third body in the triple system. The 46-d period in 4U 1636–536 was significantly detected in the *RXTE* ASM data and up to 100 keV in the BAT data, with the profile of the high-energy modulation found to be $\sim 180^\circ$ out of phase with that seen in the 1.5–12 keV band. This behaviour is inconsistent with the modulation arising solely from variable photoelectric absorption due to the precession of a warp in the accretion disc, leading us to interpret it as evidence that the high- and low-energy modulations arise from two separate yet closely linked phenomena. The appearance of the 46-d period in conjunction with the transition to the low/hard state is intriguing, leading us to speculate that this modulation could be tied to the formation of transient compact jets. In this scenario, the low-energy modulation would result from a thermal Compton component of the spectrum which varies with the accretion rate. The high-energy modulation would thus be tied to the appearance of the non-thermal hard tail arising from the formation of compact jets during episodes of decreased accretion. Further monitoring observations at radio wavelengths are being sought in order to confirm this conclusion.

ACKNOWLEDGMENTS

This work made use of quick-look results provided by the ASM/*RXTE* team. The authors thank members of the *Swift* BAT team for helpful discussions. We thank Steven Tingay for his valuable discussions and John Dickey for kindly communicating the preliminary results of the ATCA observations of 4U 1636–536. We thank the anonymous referee for their comments which improved this paper.

REFERENCES

Andrew B. H., Purton C. R., 1968, *Nat*, 218, 855
 Barret D., 2001, *Adv. Space Res.*, 28, 307
 Barthelmy S. D. et al., 2005, *Space Sci. Rev.*, 120, 143

Becker R. H., Smith B. W., Swank J. H., Boldt E. A., Holt S. S., Pravdo S. H., Serlemitsos P. J., 1977, *ApJ*, 216, L101
 Berendsen S. G. H., Fender R., Kuulkers E., Heise J., van der Klis M., 2000, *MNRAS*, 318, 599
 Bloser P. F., Grindlay J. E., Barret D., Boirin L., 2000a, *ApJ*, 542, 989
 Bloser P. F., Grindlay J. E., Kaaret P., Zhang W., Smale A. P., Barret D., 2000b, *ApJ*, 542, 1000
 Bradshaw C. F., Fomalont E. B., Geldzahler B. J., 1999, *ApJ*, 512, L121
 Byram E. T., Chubb T. A., Friedman H., 1966, *Sci*, 152, 66
 Casares J., Charles P. A., Kuulkers E., 1998, *ApJ*, 493, L39
 Casares J., Cornelisse R., Steeghs D., Charles P. A., Hynes R. I., O'Brien K., Strohmayer T. E., 2006, *MNRAS*, 373, 1235
 Corbel S., Nowak M. A., Fender R. P., Tzioumis A. K., Markoff S., 2003, *A&A*, 400, 1007
 Chou Y., Grindlay J. E., 2001, *ApJ*, 563, 934
 Chou Y., Grindlay J. E., Bloser P. F., 2001, *ApJ*, 549, 1135
 Clarkson W. I., Charles P. A., Coe M. J., Laycock S., Tout M. D., Wilson C. A., 2003a, *MNRAS*, 339, 447
 Clarkson W. I., Charles P. A., Coe M. J., Laycock S., 2003b, *MNRAS*, 343, 1213
 Corbet R. H. D., Markwardt C. B., Tueller J., 2007, *ApJ*, 655, 458
 D'Amico F., Heindl W. A., Rothschild R. E., Gruber D. E., 2001, *ApJ*, 547, L147
 Di Salvo T., Robba N., Stella L., 2002, *Mem. Soc. Astron. Ital.*, 73, 1082
 Di Salvo T. et al., 2006, *ApJ*, 649, L91
 Farrell S. A., O'Neill P. M., Sood R. K., 2005, *Pub. Astron. Soc. Aust.*, 22, 267
 Farrell S. A., Sood R. K., O'Neill P. M., Dieters S., 2008, *MNRAS*, 389, 608
 Fender R., 2006, in Lewin W., van der Klis M., eds, *Compact Stellar X-ray Sources*. Cambridge Univ. Press, Cambridge, p. 381
 Fiocchi M., Bazzano A., Ubertini P., Jean P., 2006, *ApJ*, 651, 416
 Fomalont E. B., Geldzahler B. J., Bradshaw C. F., 2001, *ApJ*, 553, L27
 Galloway D. K., Psaltis D., Muno M. P., Chakrabarty D., 2006, *ApJ*, 639, 1033
 Giacconi R., Gursky H., Paolini F., Rossi B., 1962, *Phys. Rev. Lett.*, 9, 439
 Giacconi R., Murray S., Gursky H., Kellogg E., Schreier E., Matilsky T., Koch D., Tananbaum H., 1974, *ApJS*, 27, 37
 Gottlieb E. W., Wright E. L., Liller W., 1975, *ApJ*, 195, L33
 Grindlay J. E., 1992, in Tanaka Y., Koyama K., eds, *Proc. 28th Yamada Conf., Frontiers of X-Ray Astronomy*. Universal Academy, Tokyo, p. 69
 Grindlay J. E., Gursky H., Schnopper H., Parsignault D. R., Heise J., Brinkman A. C., Schrijver J., 1976, *ApJ*, 205, L127
 Grindlay J. E., Bailyn C. D., Cohn H., Lungger P. M., Thorstensen J. R., Wegner G., 1988, *ApJ*, 334, L25
 Harmon B. A. et al., 2004, *ApJS*, 154, 585
 Hasinger G., van der Klis M., 1989, *A&A*, 225, 79
 Hoffman J. A., Lewin W. H. G., Doty J., 1977, *ApJ*, 217, L23
 Homer L., Charles P. A., Hakala P., Muhli P., Shih I.-C., Smale A. P., Ramsay G., 2001, *MNRAS*, 322, 827
 Jonker P. G., Nelemans G., 2004, *MNRAS*, 354, 355
 Kong A. K. H., Charles P. A., Kuulkers E., 1998, *New Astron.*, 3, 301
 Kuulkers E., den Hartog P. R., in't Zand J. J. M., Verbunt F. W. M., Harris W. E., Cocchi M., 2003, *A&A*, 399, 663
 Larwood J. D., Nelson R. P., Papaloizou J. C. B., Terquem C., 1996, *MNRAS*, 282, 597
 Lavagetto G. et al., 2006, *A&A*, 445, 1089
 Lewin W. H. G., Hoffman J. A., Doty J., Clark G. W., Swank J. H., Becker R. H., Pravdo S. H., Serlemitsos P. J., 1977, *Nat*, 267, 28
 Lomb N. R., 1975, *Ap&SS*, 39, 447
 Malzac J., 2007, *Ap&SS*, 311, 149
 Margon B., 1984, *ARA&A*, 22, 507
 Migliari S., Fender R. P., 2006, *MNRAS*, 366, 79
 Migliari S. et al., 2007, *ApJ*, 671, 706
 Mirabel I. F., Rodrigues I., 2003, *A&A*, 398, L25
 Ogilvie G. I., Dubus G., 2001, *MNRAS*, 320, 485
 Orosz J. A., Kuulkers E., 1999, *MNRAS*, 305, 1320

- Paul B., Kitamoto S., 2002, *JA&A*, 23, 33
- Paul B., Kitamoto S., Makino F., 2000, *ApJ*, 528, 410
- Pedersen H., van Paradijs J., Lewin W. H. G., 1981, *Nat*, 294, 725
- Peele A. G., White N. E., 1996, *IAU Circ.*, 6524
- Piraino S., Santangelo A., Kaaret P., 2002, *ApJ*, 567, 1091
- Press W. H., Rybicki G. B., 1989, *ApJ*, 338, 277
- Priedhorsky W., Terrell J., 1984a, *ApJ*, 280, 661
- Priedhorsky W., Terrell J., 1984b, *ApJ*, 284, L17
- Psaltis D., 2006, in Lewin W., van der Klis M., eds, *Compact Stellar X-ray Sources*. Cambridge Univ. Press, Cambridge, p. 1
- Rappaport S., Ma C. P., Joss P. C., Nelson L. A., 1987, *ApJ*, 322, 842
- Rutten R. G. M., van Paradijs J., Tinbergen J., 1992, *A&A*, 260, 213
- Scargle J. D., 1982, *ApJ*, 263, 835
- Scargle J. D., 1989, *ApJ*, 343, 874
- Schulz M., Mudelsee M., 2002, *Comput. Geosci.*, 28, 421
- Shih I. C., Bird A. J., Charles P. A., Cornelisse R., Tiramani D., 2005, *MNRAS*, 361, 602
- Šimon V., 2005, *A&A*, 436, 263
- Smale A. P., 1998, *ApJ*, 498, L141
- Smale A. P., Lochner J. C., 1992, *ApJ*, 395, 582
- Sood R. K., Farrell S. A., O'Neill P. M. D., Manchanda R. K., Ashok N. M., 2006, *Adv. Space Res.*, 38, 2779
- Sood R. K., Farrell S. A., O'Neill P. M. D. S., 2007, *Adv. Space Res.*, 40, 1528
- Stairs I. H., Lyne A. G., Shemar S. L., 2000, *Nat*, 406, 484
- Stella L., Priedhorsky W., White N. E., 1987, *ApJ*, 312, L17
- Swank J. H., Taam R. E., White N. E., 1984, *ApJ*, 277, 274
- Strickman M., Barret D., 2000, in McConnell M. L., Ryan J. M., eds, *AIP Conf. Proc.* 510, Proc. 5th Compton Symp. Am. Inst. Phys., Melville, p. 222
- Tarana A., Bazzano A., Ubertini P., Zdziarski A. A., 2007, *ApJ*, 654, 494
- Trümper J., Kahabka P., Ögelman H., Pietsch W., Voges W., 1986, *ApJ*, 300, L63
- Vanderlinde K. W., Levine A. M., Rappaport S. A., 2003, *PASP*, 115, 739
- Weiler K. W., van Dyk S. D., Pringle J. E., Panagia N., 1992, *ApJ*, 399, 672
- Wen L., Levine A. M., Corbet R. H. D., Bradt H. V., 2006, *ApJS*, 163, 372
- White N. E., Swank J. H., 1982, *ApJ*, 253, L61
- Wijers R. A. M., Pringle J. E., 1999, *MNRAS*, 308, 207
- Wijnands R. A. D., Kuulkers E., Smale A. P., 1996, *ApJ*, 473, L45
- Zdziarski A. A., Wen L., Gierliński M., 2007a, *MNRAS*, 377, 1006
- Zdziarski A. A., Gierliński M., Wen L., Kostrzewa Z., 2007b, *MNRAS*, 377, 1017
- Zhang W., Smale A. P., Strohmayer T. E., Swank J. H., 1998, *ApJ*, 500, L171

APPENDIX A: LIGHT CURVES

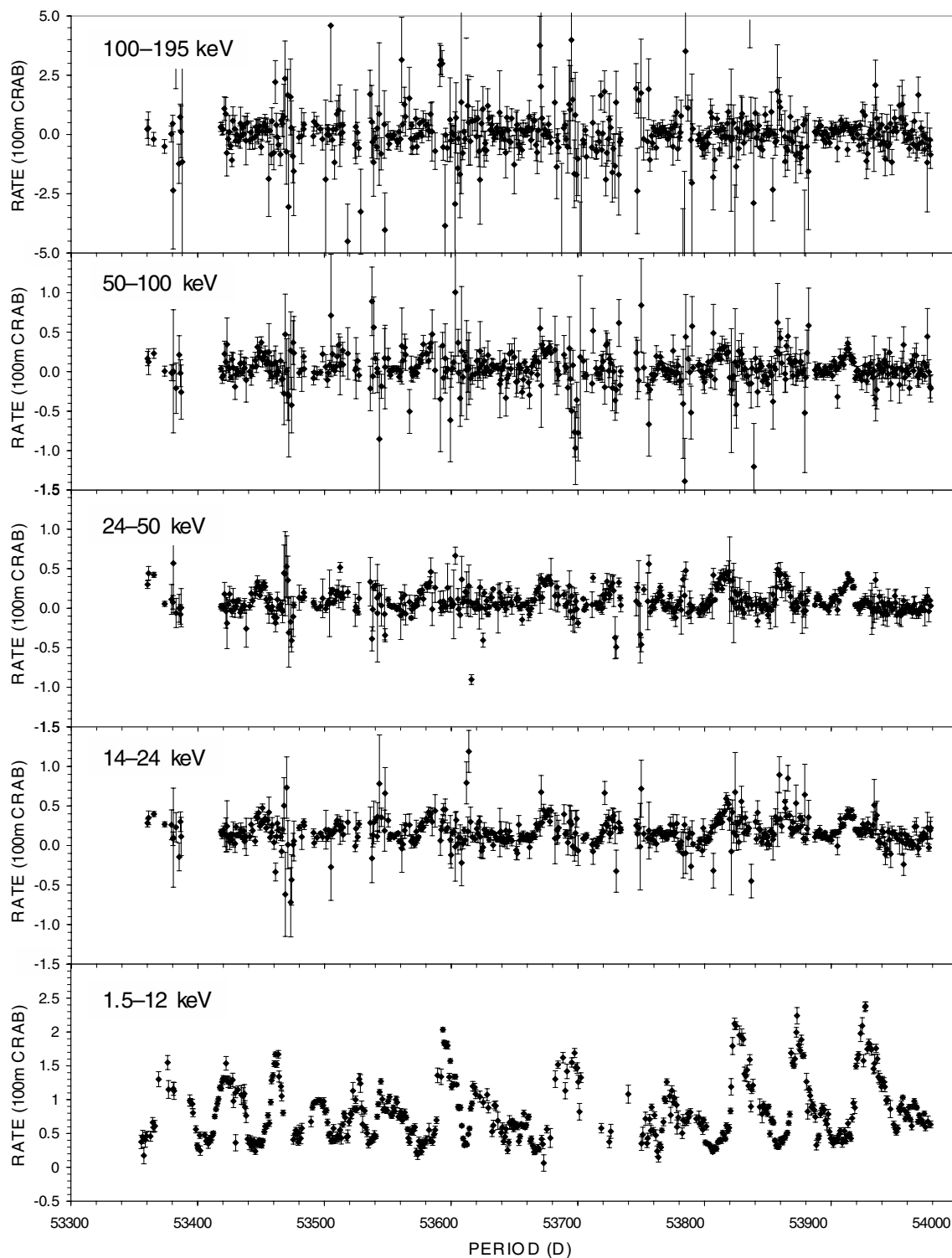


Figure A1. 4U 1636–536: the 1.5–12 keV *RXTE* ASM light curve (bottom panel) and the 14–24, 24–50, 50–100 and 100–195 keV *Swift* BAT light curves (top panels).

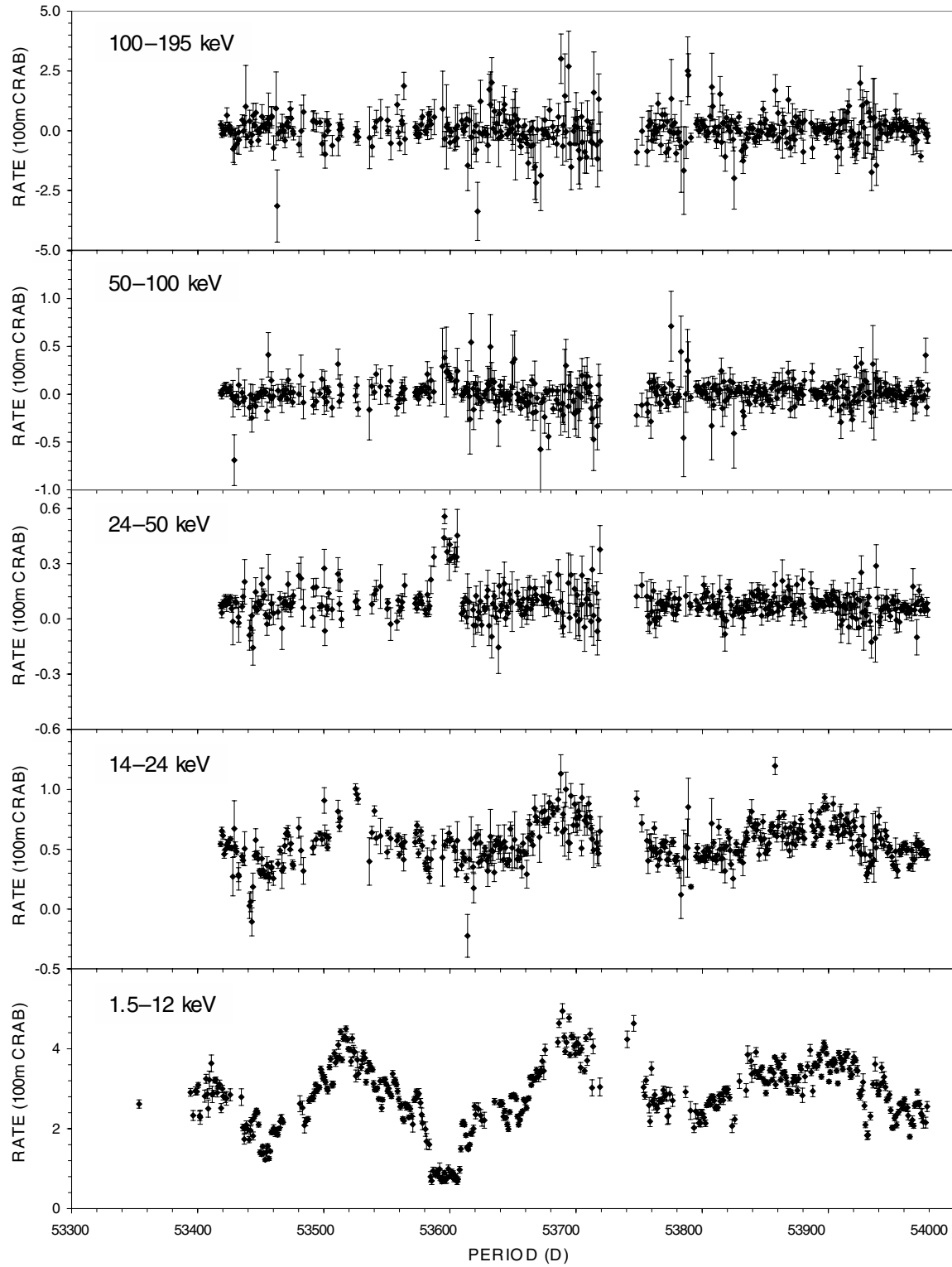


Figure A2. 4U 1820–303: the 1.5–12 keV *RXTE* ASM light curve (bottom panel) and the 14–24, 24–50, 50–100 and 100–195 keV *Swift* BAT light curves (top panels).

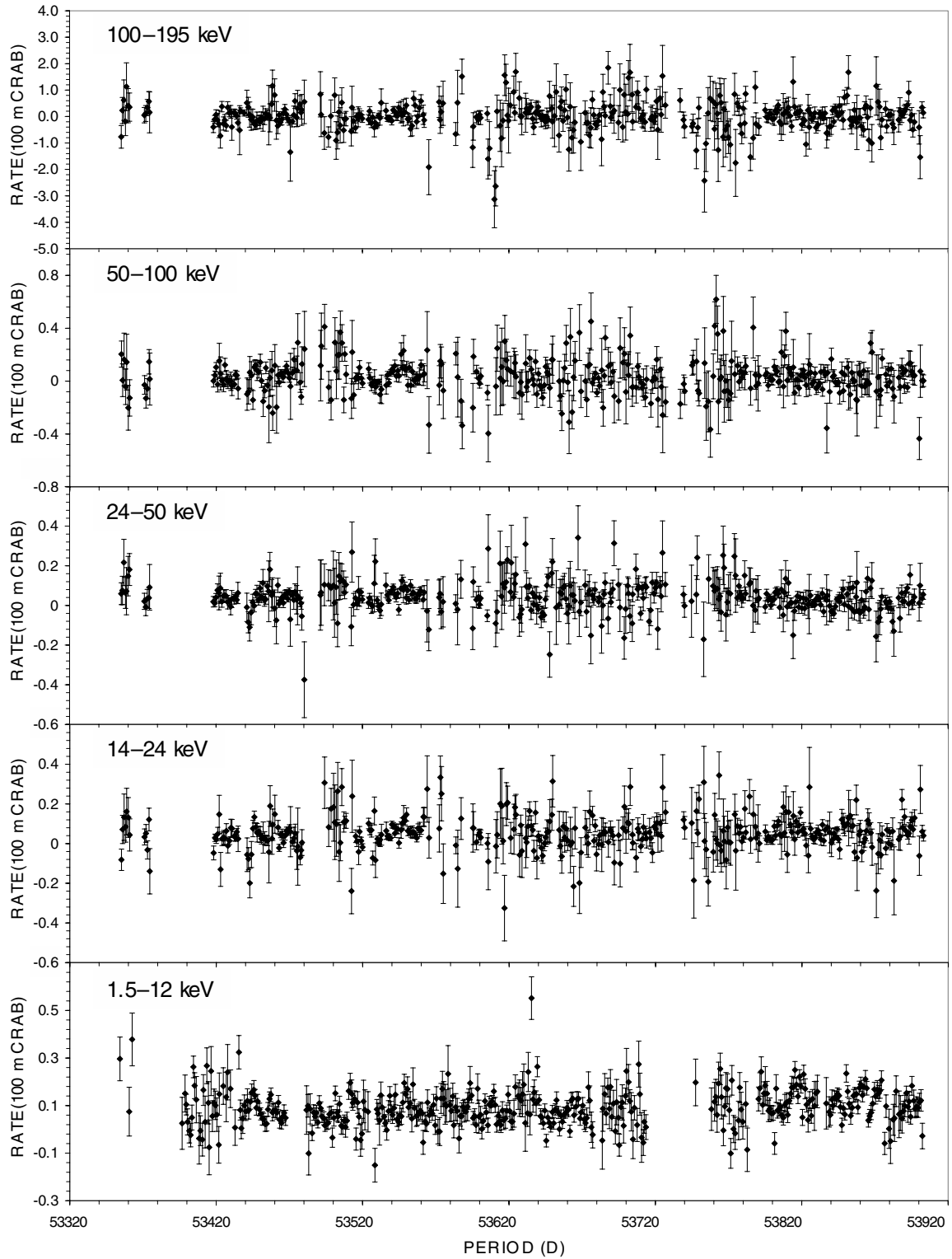


Figure A3. 4U 1916–053: the 1.5–12 keV *RXTE* ASM light curve (bottom panel) and the 14–24, 24–50, 50–100 and 100–195 keV *Swift* BAT light curves (top panels).

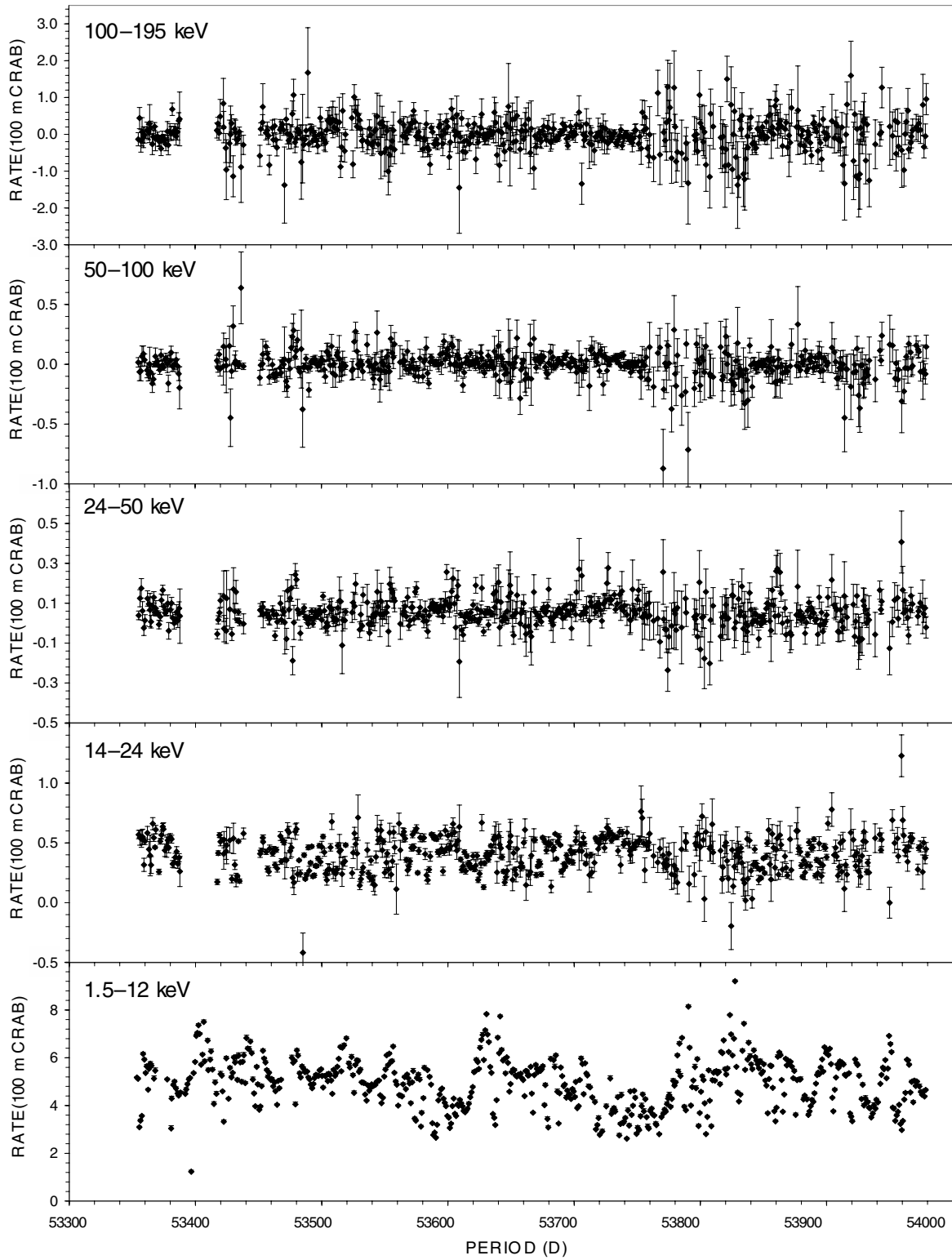


Figure A4. Cyg X-2: the 1.5–12 keV *RXTE* ASM light curve (bottom panel) and the 14–24, 24–50, 50–100 and 100–195 keV *Swift* BAT light curves (top panels).

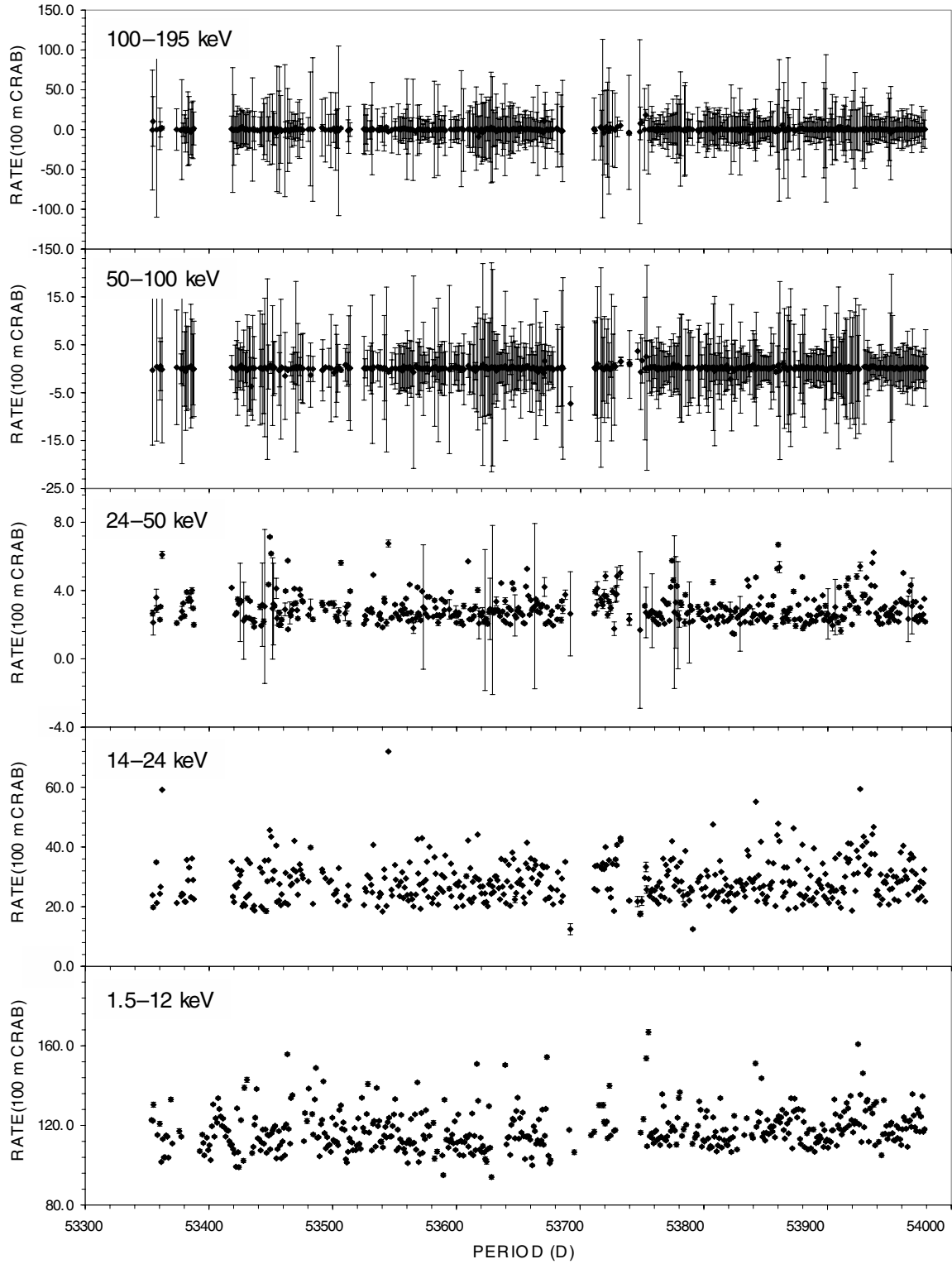


Figure A5. Sco X-1: the 1.5–12 keV *RXTE* ASM light curve (bottom panel) and the 14–24, 24–50, 50–100 and 100–195 keV *Swift* BAT light curves (top panels).

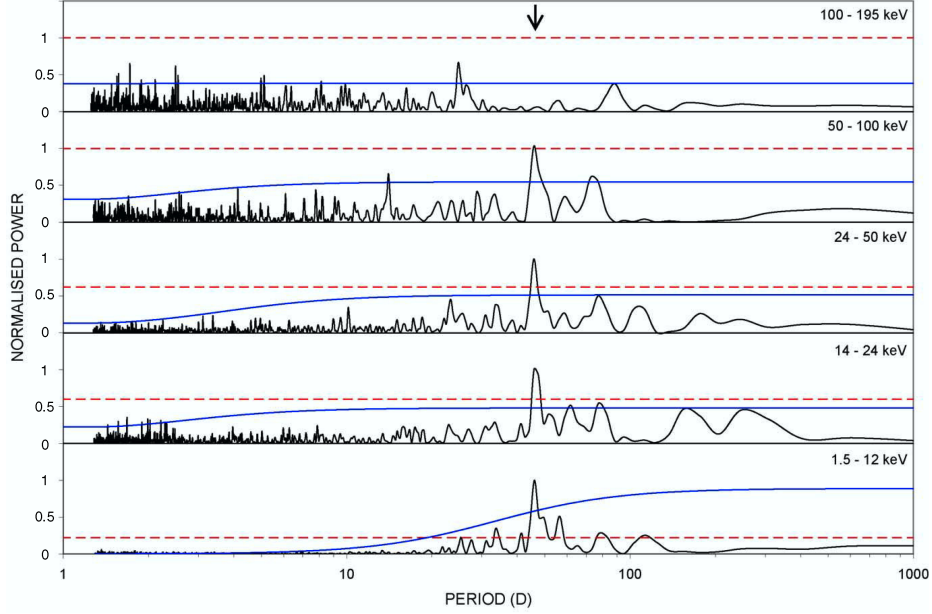
APPENDIX B: POWER SPECTRA

Figure B1. 4U 1636–536: normalized power spectra of the 1.5–12 keV *RXTE* ASM light curve (bottom panel) and the 14–24, 24–50, 50–100 and 100–195 keV *Swift* BAT light curves (top panels). The red horizontal dashed lines and blue solid lines indicate the 99 per cent white and red noise significance levels, respectively. The arrow indicates the location of the previously reported superorbital period of 46 d. The power spectra were each normalized to the maximum power present, the 99 per cent white or red noise levels, whichever was greatest.

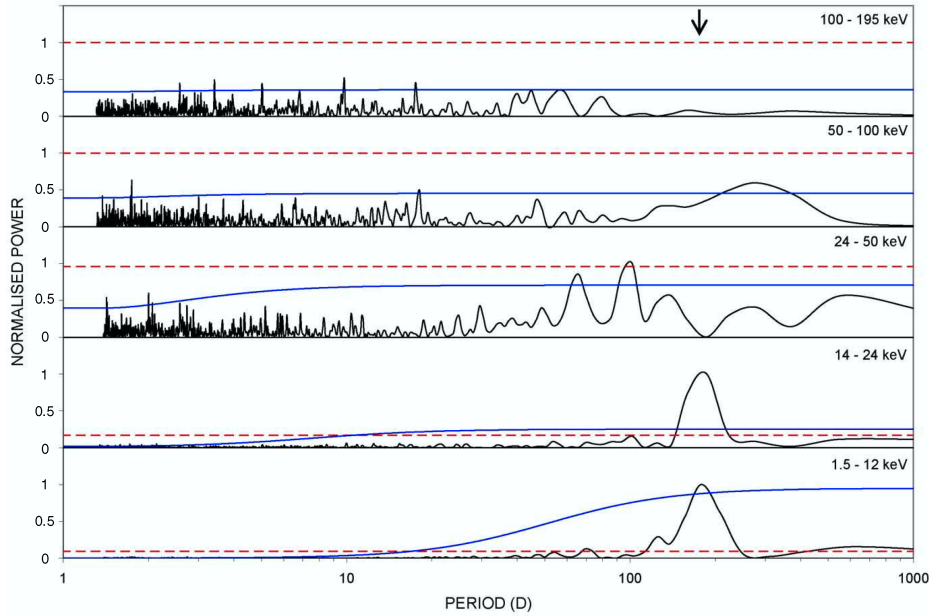


Figure B2. 4U 1820–303: normalized power spectra of the 1.5–12 keV *RXTE* ASM light curve (bottom panel) and the 14–24, 24–50, 50–100 and 100–195 keV *Swift* BAT light curves (top panels). The arrow indicates the location of the previously reported superorbital period of ~ 170 d.

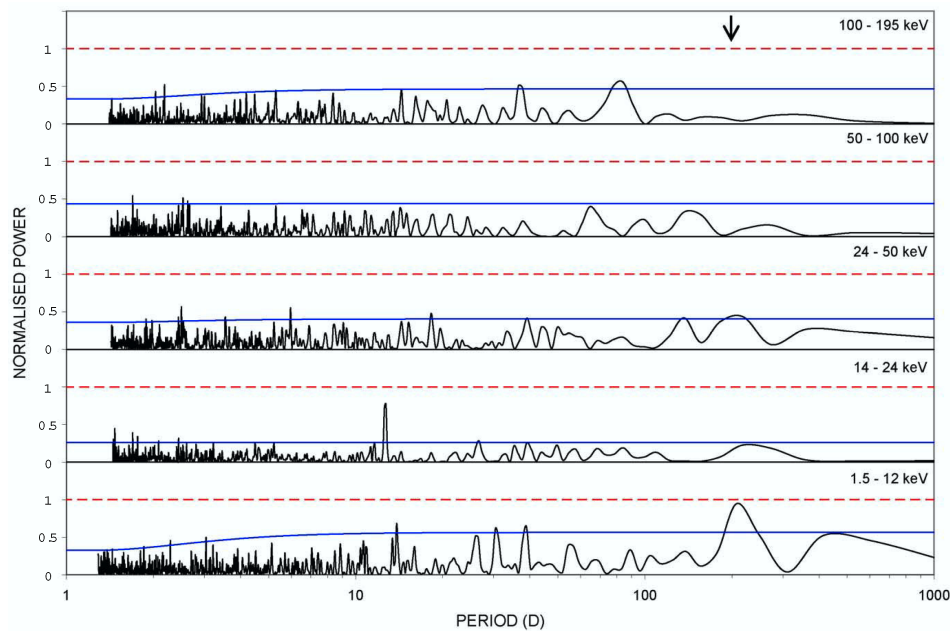


Figure B3. 4U 1916–053: normalized power spectra of the 1.5–12 keV *RXTE* ASM light curve (bottom panel) and the 14–24, 24–50, 50–100 and 100–195 keV *Swift* BAT light curves (top panels). The arrow indicates the location of the previously reported superorbital period of 199 d.

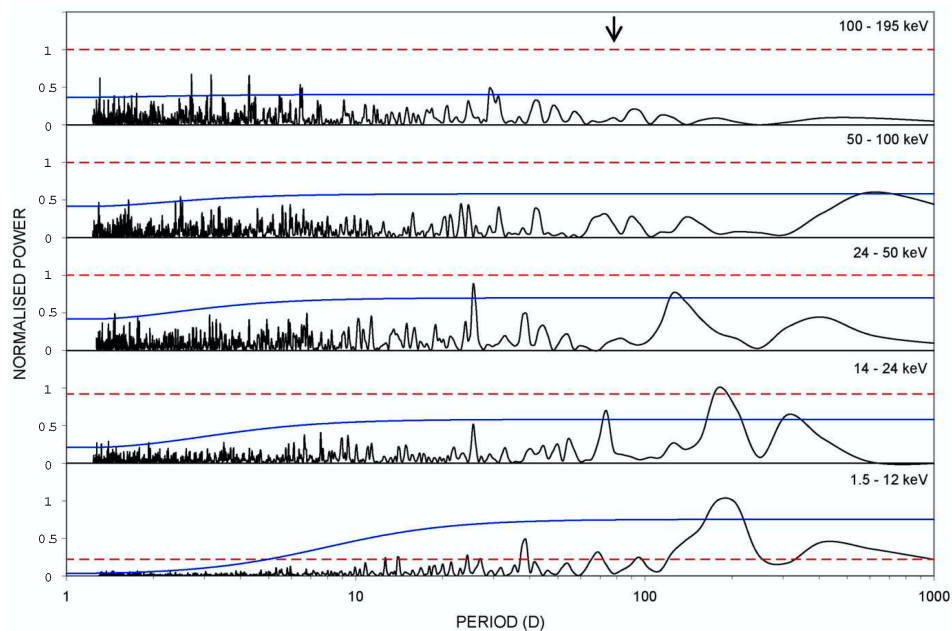


Figure B4. Cyg X-2: normalized power spectra of the 1.5–12 keV *RXTE* ASM light curve (bottom panel) and the 14–24, 24–50, 50–100 and 100–195 keV *Swift* BAT light curves (top panels). The arrow indicates the location of the previously reported superorbital period of 78 d.

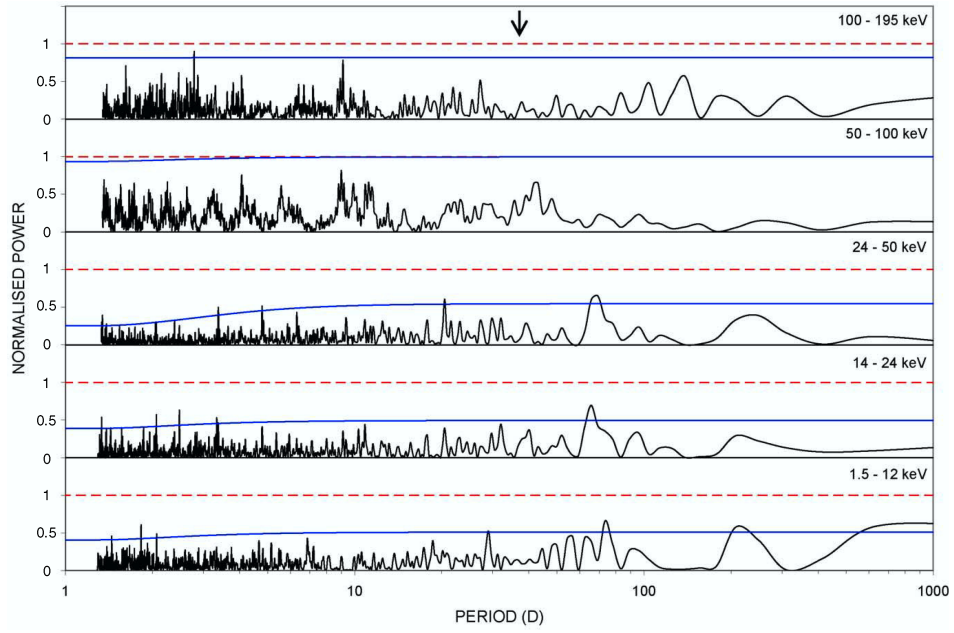


Figure B5. Sco X-1: normalized power spectra of the 1.5–12 keV *RXTE* ASM light curve (bottom panel) and the 14–24, 24–50, 50–100 and 100–195 keV *Swift* BAT light curves (top panels). The arrow indicates the location of the previously reported superorbital periods of 37 d.

This paper has been typeset from a \LaTeX file prepared by the author.